Top Organomet Chem (2019) 64: 77–100
DOI: 10.1007/3418_2018_9

Published online: 10 June 2018

Cobalt(II)/(III)–Lanthanide(III) Complexes as Molecular Magnets

Atanu Dey, Shalini Tripathi, Maheswaran Shanmugam, Ramakirushnan Suriya Narayanan, and Vadapalli Chandrasekhar

Contents

Abstract This chapter deals with single-molecule magnets (SMMs) obtained from heterometallic Co(II)/4f complexes. The design principles involved in building various types of heterometallic complexes are discussed along with their magnetic properties. A large group of hybrid Co(II)/4f complexes of varying nuclearity are discussed. Some examples of Co(III)/4f complexes are also presented.

Keywords Cluster complexes · Cobalt/lanthanide complexes · Lanthanides · Magnetism · Single molecule magnet · Slow relaxation of magnetization

---

The original version of this chapter was revised. A correction to this chapter is available at DOI 10.1007/3418_2019_33.

All the authors contributed equally to this work.

A. Dey and R. S. Narayanan
Tata Institute of Fundamental Research Hyderabad, Hyderabad, India

S. Tripathi and M. Shanmugam
Department of Chemistry, Indian Institute of Technology Bombay, Mumbai, Maharashtra, India

V. Chandrasekhar (✉)
Tata Institute of Fundamental Research Hyderabad, Hyderabad, India

Department of Chemistry, Indian Institute of Technology Kanpur, Kanpur, Uttar Pradesh, India
e-mail: vc@tifrh.res.in; vc@iitk.ac.in

1 Introduction

In the previous chapter while discussing the complexes containing Co(II)-based SMMs/SIMs, it was noted that the ground state *S* value is fixed, and the *D* value is the sole parameter to fine-tune the magnetic behavior. Because of factors such as (1) the small and fixed "*S*" value associated with Co(II) ions, (2) quenching of orbital angular momentum due to the ligand field, (3) ligand-induced structural distortion, and (4) nuclear hyperfine interaction, faster relaxation mechanism such as QTM can become operative in homometallic Co(II) complexes [1–3]. To some extent, these factors can be overcome by employing multidentate ligand or compartmental ligand to link Co(II) along with other suitable lanthanide ions simultaneously in a heterometallic ensemble. This will be the focus of this chapter.

The first lanthanide-based SMM in 2003, a mononuclear [Pc_2Tb] complex, phthalocyanine (Pc), has attracted a great interest toward the use of lanthanide ions in SMMs [4]. Accordingly, the first heterometallic SMM, a Cu_2Tb_2 complex, was reported in 2004 [5]. The heterometallic tetrameric complex was isolated by the reaction of K[CuL] and [$Tb^{III}(hfac)_3(H_2O)_2$] (**1**) where H_3L = 1-(2-hydroxybenzamido)-2-(2-hydroxy-3-methoxy-benzylideneamino)-ethane. The crystal structure of the complex with molecular formula [$Cu^{II}LTb^{III}(hfac)_2]_2$ is shown in Fig. 1. Instead of the $[CuL]^-$ precursor, if the analogous $[NiL]^-$ precursor [$Ni^{II}LTb^{III}(hfac)_2]_2$ (**2**) is used, where the paramagnetic Cu(II) ion was replaced with diamagnetic Ni^{II} affording an opportunity to compare the role of Cu(II) ion in **1**.

Complex **1** shows ferromagnetic interaction between the Cu^{II} and Tb^{III} ions with a positive Weiss constant (θ = +14.3 K) as originally proposed by Gatteschi and co-workers [6]. Complex **1** showed SMM behavior [$(\tau_0) = 2.7 \times 10^{-8}$ s; $U_{eff} = \Delta/k_B$) = 21 K; T_B = 1.2 K). However, hysteresis was not observed at the measured temperatures, viz., above 2 K.

Under similar condition, complex **2** reveals a simple paramagnetic behavior that may be due to the magnetic anisotropy and/or intermolecular antiferromagnetic interaction and/or dipolar interaction. AC susceptibility measurement of **2** does not display χ_M'' signal which may be due to the fast QTM at zero magnetic field. Possibly the presence of ferromagnetic exchange interaction between Cu(II) and Tb(III) ion is likely the reason for the observed SMM behavior in **1** ($H_{DC} = 0$).

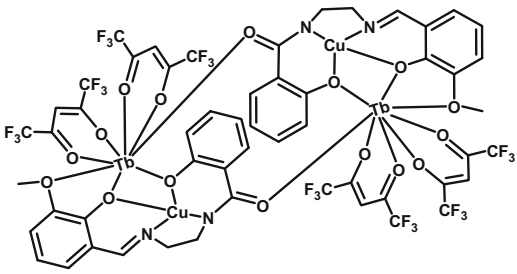

Fig. 1 Line diagram of **1**

Based on these early forays, the advantage of using 3d–4f heterometallic complexes were reasoned as: (1) relatively high spin ground state can be achieved using less number of metal ions compared to larger polynuclear 3d metal complexes, and (2) anisotropy can be harvested through the lanthanide ions by exploiting its unquenched orbital angular momentum.

Presence of QTM is a major problem in incorporating lanthanide ion although the single-ion magnetic anisotropy of these ions is generally large as compared to the 3d metal ions. Due to this fact, the blocking temperature remains well below 5 K in majority of the 3d–4f metal complexes [7]. However, this disadvantage can be minimized by enhancing the exchange interaction between 3d and 4f ions. This phenomenon was first reported by Murray and co-workers by enhancing the exchange interaction between the Cr(III) and Dy(III) ion in a heterometallic $[Cr^{III}_2Ln^{III}_2(OMe)_2(mdea)_2(O_2CPh)_4(NO_3)_2]$ (**3**), Ln^{III} = Pr, Nd, Gd, Tb, Ho, and Er and mdea = *N*-methyl diethanolaminato(2−) butterfly complex where QTM is significantly reduced/quenched which facilitate in enhancing the blocking temperature [8, 9]. Due to the arrest/quenching of magnetization, opening of a hysteresis loop is generally observed unlike in transition metal clusters (Fig. 2). Similarly, heterometallic Ni_2Dy_2(**4**) complex is found to show a similar behavior, where

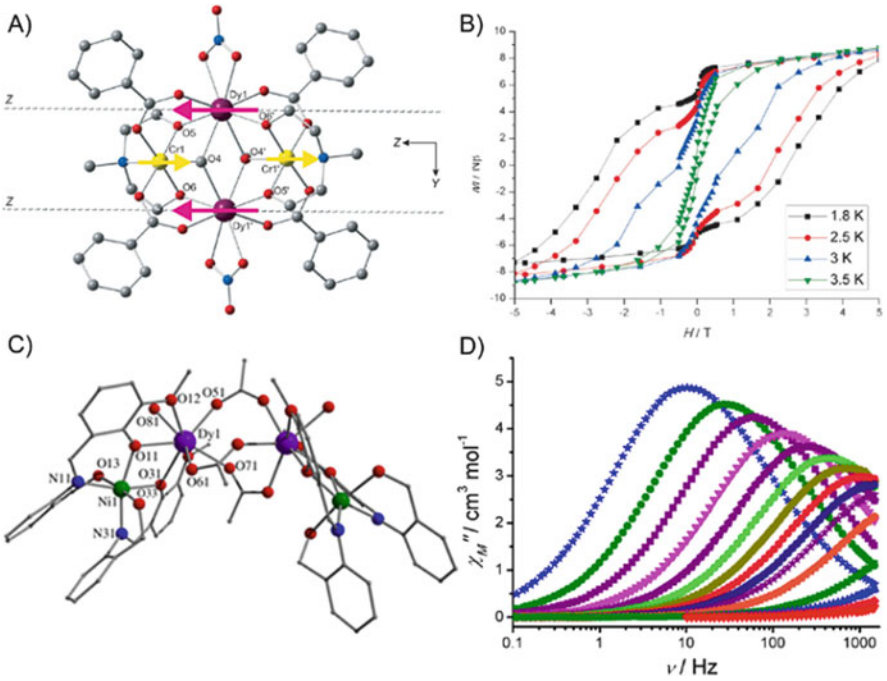

Fig. 2 (**a**) Ball and stick presentation of **3**. (**b**) Magnetization vs field plot with a sweep rate of 0.003 Ts^{-1}. Adapted from *Angew. Chem. Int. Ed.* **2013**, *52*, 12014 with permission from John Wiley and Sons. (**c**). Ball and stick presentation of **4**. (**d**) Frequency-dependent AC susceptibility measurements performed on polycrystalline sample of **4**. Adapted from *Chem. Eur. J,* **2014**, *20*, 14235 with permission from John Wiley and Sons

QTM is found to be suppressed completely resulting in a zero-field SMM [10]. The anisotropic barrier extracted for the later complex (19 cm^{-1}) in zero applied DC magnetic field, and the one estimated in the presence of external magnetic field (18.9 cm^{-1}) is found out to be similar indicating that QTM is efficiently suppressed. In both cases (Cr_2Dy_2 and Ni_2Dy_2), quenching of QTM is attributed to the presence of enhanced exchange interaction compared to the other 3d–4f complexes reported in the literature. Further, it has been proposed that a larger ∠Ni–O–Dy angle and smaller distortion in the dihedral plane formed by Ni–O–Dy–O are the recipe for increasing the ferromagnetic exchange.

The presence of 3d ion in near vicinity of Ln(III) ion environment is not the only option, but paramagnetic bridging ligands can play a crucial role in increasing the exchange interaction. This has been elegantly proven in a series of Ln_2 dimers linked through unusual N_2^{3-} radical ligand (with a blocking temperature of 14 K for the Tb_2 analogue) [11, 12].

Since several 3d–4f metal complexes are known in the literature, we will restrict to Co(II)/4f SMM reported in the literature in this chapter. We will also discuss some examples of Co(III)/4f complexes. Before this a brief introduction on the nature of interaction between the 3d and 4f metal ions is in order.

To ascertain qualitatively the nature of exchange interaction between the 3d and the 4f metal ion, Andruh et al. proposed an empirical approach by considering Ni–Ln (Ln = Dy or Pr) dimeric complexes [13]. In such complexes, the total magnetic moment experimentally observed is the combination of magnetic moment contribution from individual metal ions (e.g., nickel and Ln(III) ion) along with the exchange couple state. Hence, by subtracting the individual metal ion contribution from the total magnetic moment, the masked nature of interaction will be clearly reflected by plotting the temperature-dependent $\Delta\chi_M T$ value.

The empirical equation is

$$\Delta\chi_M T = \chi_M T_{Ni,Dy} - \chi_M T_{Zn,Dy} - \chi_M T_{Ni,Lu} = \sim J_{Ni-Dy}$$

For example, the presence of ferromagnetic exchange interaction observed between Ni(II) and Dy(III) complexes in Ni_2Dy_2 tetrameter is revealed using the empirical equation shown above.

For a system with ferromagnetic interaction, the $\Delta\chi_M T$ plot will raise at low temperature in positive direction, while for an antiferromagnetic interaction, the plot will plunge into negative $\Delta\chi_M T$ value. The general trend noticed in case of Cu(II)–Ln or Ni(II)–Ln complexes are: (1) a ferromagnetic exchange interaction is observed if Ln (III) valence shell contains $\geq f^7$ electrons, and (2) an antiferromagnetic coupling exists if Ln(III) valence shell electron become less than 7. This scenario is witnessed in many such complexes, which is very well exemplified [13]. We have noticed recently that a similar trend is also observed in Co(II) containing 4f complexes. Hence, targeting Co (II)–Ln(III) (where $Ln^{III} \geq f^7$) is an ideal approach to reveal a new generation of SMMs. Accordingly, various Co(II)/(III)–Ln(III) SMMs reported in literature have been overviewed below.

2 Hybrid Co–4f Complexes as SMMs

This section deals with various examples on heterometallic Co(II)/Ln(III) and Co (III)/Ln(III) complexes. In the case of Co(III)/Ln(III) complexes, the magnetic properties are entirely due to the lanthanide ion.

Based on the above insight, several heterometallic 3d/4f complexes were investigated [7, 14–23]. The first Co/Ln SMM, $[L_2Co^{II}{}_2Gd][NO_3]$ (**5**), was reported by Chandrasekhar and co-workers. The complex was assembled using a phosphorus-based tris-hydrazone ligand (LH_3) and contains a linear array of metal ions [24] (Fig. 3).

The zero-field SMM behavior of this complex was confirmed by AC susceptibility measurements (Fig. 4): $U_{eff} = 27.2$ K and $\tau_0 = 1.7 \times 10^{-7}$ s.

Several other structurally analogous trinuclear complexes $\{[L_2Co^{II}{}_2Ln][X]\}$ [Ln = Eu, X = Cl; Ln = Tb, Dy and Ho, X = NO_3] were also prepared, all of which except the Eu^{III} analogue were shown to be SMMs [25]. Table 1 summarizes the magnetic data for all of these complexes.

Following these first examples, there have been several studies on such heterometallic Co(II)/Ln(III) and Co(III)/Ln(III) complexes. In the subsequent sections, we will discuss these based on the nuclearity of the complexes. Only such complexes will be discussed where there has been a demonstration of SMM behavior.

2.1 Dinuclear Complexes

The preparation of the heterometallic complexes discussed in this and subsequent sections is dependent on the use of the so-called compartmental ligands which have specificity toward either the transition metal ion or the lanthanide metal ion.

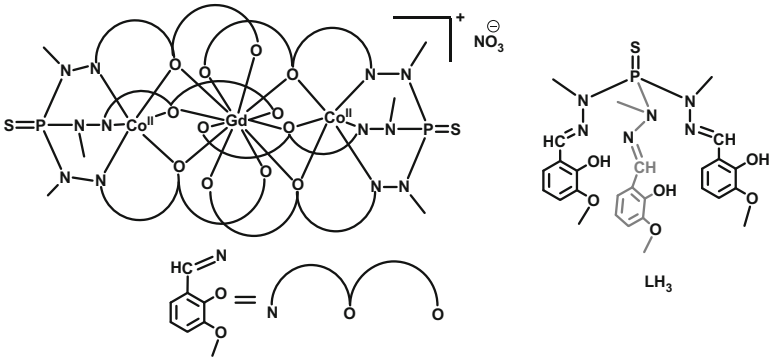

Fig. 3 Line diagram of **5** along with the ligand

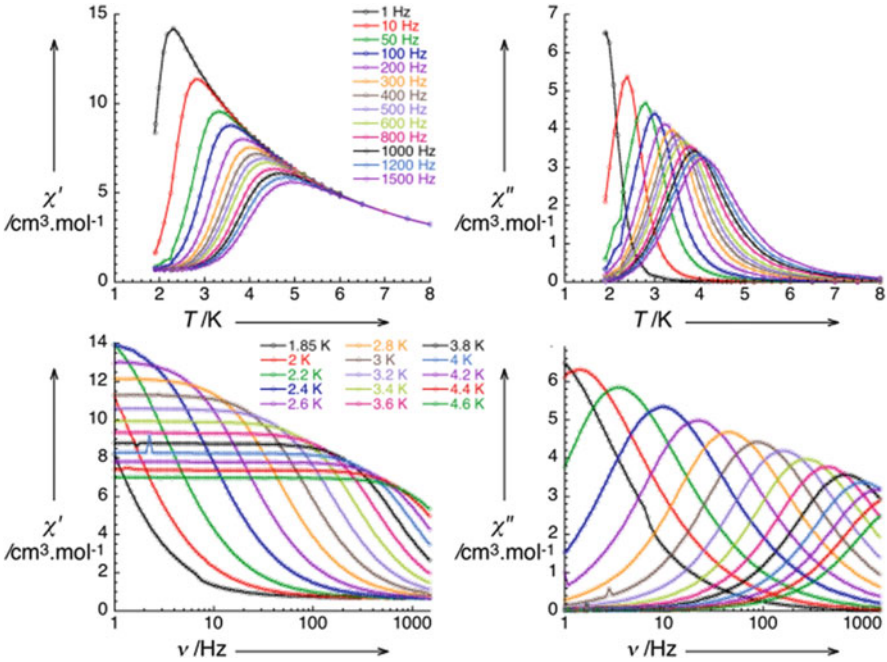

Fig. 4 Temperature (top) and frequency (bottom) dependence of the in-phase and out-of-phase AC susceptibility measurements under zero applied DC field. Reprinted with permission from (*Inorg Chem.* **2009**, *48*, 1148–1157), Copyright (2009) American Chemical Society

Table 1 Magnetic data for $[L_2Co^{II}{}_2Ln]^+$ SMMs

Complex	U_{eff} (K), τ_0 (s) at $H_{DC} = 0$	U_{eff}(K), τ_0 (s) at $H_{DC} \neq 0$
$[L_2Co^{II}{}_2Gd][NO_3]$ (**5**)	27.2, 1.7×10^{-7}	27.4, 1.5×10^{-7}, 1,000 Oe
$[L_2Co^{II}{}_2Tb][NO_3]$ (**6**)	18.9, 5.5×10^{-6}	25.8, 3.7×10^{-6}, 1,500 Oe
$[L_2Co^{II}{}_2Dy][NO_3]$ (**7**)	14.2, 5.1×10^{-6}	–
$[L_2Co^{II}{}_2Ho][NO_3]$ (**8**)	8, 13×10^{-5}	–

A cyanido-bridged complex, $[\{Dy^{III}(3\text{-OHpy})_2(H_2O)_4][Co^{III}(CN)_6\}]$ (**9**), was reported by the self-assembly reaction involving Dy^{III}–3-hydroxypyridine (3-OHpy) complexes with hexacyanidocobaltate(III). This complex, which can be considered as single-ion magnet, shows SMM behavior with a high U_{eff} of 266 cm^{-1} (≈385 K) and a $\tau_0 = 3.2 \times 10^{-11}$ s above 23 K at $H_{DC} = 0$ Oe. Moreover, magnetization hysteresis loops are observed below 6 K with a field sweep rate of 10 Oe s^{-1} [26].

In contrast to the above, a Co^{II}/Y^{III} complex, $[Co^{II}(\mu\text{-L})(\mu\text{-OAc})Y(NO_3)_2]$ (**10**), was prepared using a compartmental ligand *N*,*N*′,*N*″-trimethyl-*N*,*N*″-bis(2-hydroxy-3-methoxy-5-methylbenzyl)diethylenetriamine (H_2L) [27] (Fig. 5).

Although these complexes do not show zero-field SMM behavior, AC measurements at $H_{DC} = 1{,}000$ Oe revealed them to be SMMs. An effort was made to

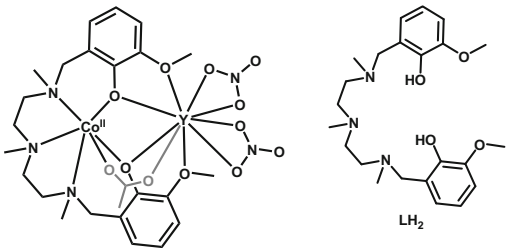

Fig. 5 Line diagram of the complex **10** along with the ligand

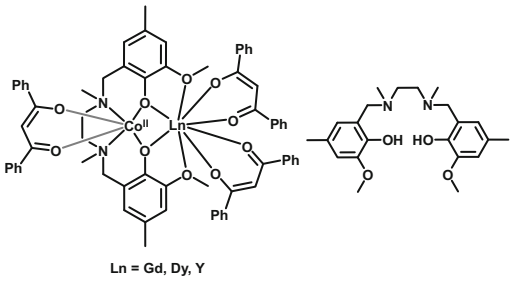

Fig. 6 Line diagram of complexes **11**−**13** along with the ligand

modulate the structural features by varying the bridging ligand which did not result in any significant change in the magnetic properties. An interesting aspect of these complexes is that all of them have been shown to have a positive D and in spite of this they exhibit a field-induced SMM behavior, rather intriguingly [28]. Rationale for the observation of field-induced slow relaxation of magnetization with easy plane anisotropy was explained in the previous chapter.

Another family of dinuclear Co–Ln complexes, $[Co^{II}Ln^{III}(L)(DBM)_3]$ [Ln = Y (**11**), Dy (**12**) and Gd (**13**)], is known; the ligands used were *N*,*N*′-dimethyl-*N*, *N*′-(2-hydroxy-3-methoxy-5-methyl-benzyl)ethylenediamine (LH_2) and the anion of 1,3-diphenyl-propane-1,3-dione (DBM^-) [29] (Fig. 6).

These complexes also reveal a positive D ($S = 3/2$, $g = 2.39$, $D = 10.3\ cm^{-1}$ and $E = 4 \times 10^{-4}\ cm^{-1}$ for Co^{II}−Y analogue); the latter reveals a field-induced single-molecule magnet (SMM) behavior (Fig. 7).

M^{II}−Ln binuclear complexes, $[M^{II}(3\text{-MeOsaltn})(MeOH)(OAc)Ln(hfac)_2]$ (M^{II} = Co, Ni, Cu and Zn; Ln = Gd^{III}, Tb^{III}, Dy^{III}, La^{III}) were prepared by using *N*, *N*′-bis(3-methoxy-2-oxybenzylidene)-1,3-propanediaminato (3-MeOsaltn) and hexafluoroacetylacetonato (hfac) [30]. The M^{II}−Ln magnetic interactions are ferromagnetic when M^{II} = (Cu^{II}, Ni^{II}, and Co^{II}) and Ln = (Gd^{III}, Tb^{III}, and Dy^{III}). The D value was found to be positive for the Co^{II}/La analogue. These complexes however did not display zero-field SMM behavior.

Table 2 summarizes the magnetic data for some dinuclear Co(II)/Ln(III) complexes.

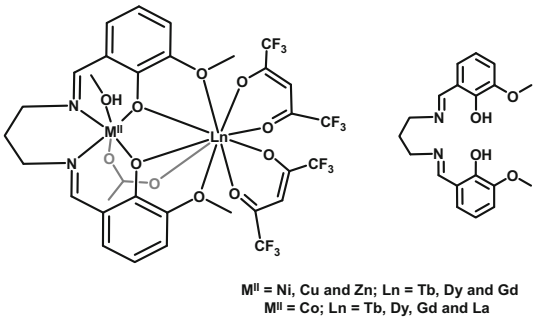

Fig. 7 Line diagram of complexes **14** and **15** and the corresponding ligand

Table 2 Magnetic properties of dinuclear [Co–Ln] SMMs

Molecular formula[a]	U_{eff} (K), H_{DC} (Oe)	τ_0 (s)	Ref.
$[Co^{II}Dy(hfac)_3(hfac)_2(NIT\text{-}3py)_2]$ (**16**)	3.61, 2000	3.09×10^{-6b}	[31]
$[Co^{II}Y^{III}(\mu\text{-}L)(\mu\text{-}NO_3)(NO_3)_2]$ (**17**)	23.9	1.5×10^{-6}	[28]
$[Co^{II}Y^{III}(\mu\text{-}L)(\mu\text{-}OAc)(NO_3)_2]$ (**10**)	27.1	4.05×10^{-7}	[27]
$[Co^{II}Tb(3\text{-}MeOsaltn)(MeOH)(OAc)(hfac)_2]$ (**18**)	17, 1,000	6.1×10^{-8}	[30]
$[Ni^{II}Tb(3\text{-}MeOsaltn)(MeOH)(OAc)(hfac)_2]$ (**19**)	14.9, 1,000	2.1×10^{-7}	[30]
$[Co^{III}Dy(HL^{SB})(AcO)_3(H_2O)_3]\cdot(AcO)$ (**20**)	113, 2,000	7.0×10^{-9}	[32]
$Co^{III}DyL^1(\mu\text{-}OAc)_2(NO_3)_2]$ (**21**)	17.6, 1,000	2.53×10^{-6}	[33]
	25.9, 2,000	4.67×10^{-7}	
	29.5, 3,000	1.14×10^{-7}	

[a]*NIT-3py* 2-(3-pyridyl)-4,4,5,5-tetramethylimidazoline-1-oxyl-3-oxide, *hfac* hexafluoroacetylacetonate, *SB* Schiff base condensation between 2-hydroxy-1,3-diaminopropane and *o*-vanillin, L^IH_2 *N,N′*-ethylenebis(3-ethoxysalicylaldimine), H_2L *N,N′,N″*-trimethyl-*N,N″*-bis (2-hydroxy-3-methoxy-5-methylbenzyl)diethylenetriamine

[b]$\ln(\chi''/\chi') = \ln(\omega\tau_0) + \Delta_{eff}/k_BT$ [34]

2.2 Trinuclear Cobalt–Lanthanide SMMs

In contrast to the trinuclear complexes described above involving a phosphorus-supported ligand, another series, $[Co^{III}{}_2Dy(L)_2(\mu\text{-}O_2CCH_3)_2(H_2O)_3](NO_3)$ (**22**) (LH_3 = 2-methoxy-6-[{2-(2-hydroxyethylamino)ethylimino}-methyl]phenol), is known. This complex showed slow relaxation of magnetization at 1,000 Oe applied DC field [$(U/k_B) = 88$ K; $(\tau_0) = 1.0 \times 10^{-8}$ s) [35] (Fig. 8).

In these examples, the analogous Tb(III) complex (**23**) has a lower $U_{eff} = 15.6$ K. It has been suggested that this may be due to the fact that while Dy(III) is a Kramers ion, the integer m_j level of Tb(III) is likely to trigger the ground state tunneling [36].

$[Co^{II}Ln_2{}^{III}]$ complexes, $[Ln^{III}{}_2Co^{II}(C_7H_5O_2)_8]$ [Ln = Dy (**24**) and Tb (**25**)] containing an in situ generated salicylaldehyde as the ligand, have been prepared [37] (Fig. 9).

Both **24** and **25** display SMM behavior at zero DC field, although **25** does not show a clear maxima in the χ'' vs T plot. For **24**, two relaxation processes could be

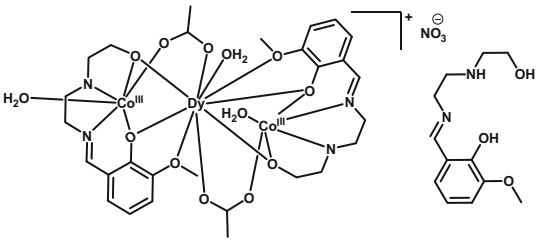

Fig. 8 Line diagram of **22** and the corresponding ligand

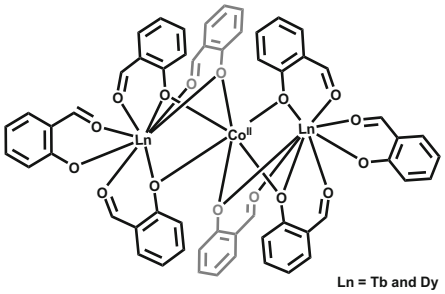

Fig. 9 Line diagram of complexes **24** and **25**

delineated: relaxation at the higher temperature region (above 5 K) being suggested as being associated with the excited Kramer doublets of individual Dy^{III} ions, while at the low temperature region (below 5 K), the weak coupling between Co^{II} and Dy^{III} appears to predominate [38].

Complexes containing Co(III), $[Co^{III}{}_2Dy(hmb)_2(CH_3O)_2(OAc)_3]$ [Ln = Dy (**26**) and Lu (**27**)], could be prepared using 2-hydroxy-3-methoxybenzylidene benzohydrazide (H_2hmb) [39] (Fig. 10).

Frequency-dependent AC susceptibility measurements for **26** at 500 Oe applied DC field provide the energy barrier (U_{eff}) = 5.5 K and $\tau_0 = 2.7 \times 10^{-5}$ s.

The magnetic properties of trinuclear Co(II)/Ln(III) and Co(III)/Ln(III) SMMs are summarized in Table 3.

2.3 Tetranuclear Cobalt–Lanthanide SMMs

A $[Co^{II}{}_2Dy_2(L)_4(NO_3)_2(THF)_2]$ (**39**) complex having a butterfly/defect-dicubane topology was assembled using 2-[(2-hydroxy-phenylimino)-methyl]-6-methoxyphenol) (H_2L) [45] (Fig. 11).

Analysis of the frequency-dependent AC measurements in zero DC field revealed the presence of two thermally activated relaxation regimes [(U_{eff}) of 11.0 cm^{-1} (15.8 K); $\tau_0 = 7.7 \times 10^{-4}$ s in the temperature range 1.6–8 K and (U_{eff}) of 82.1 cm^{-1} (118.12 K); $\tau_0 = 6.2 \times 10^{-7}$ s between 18 and 22 K]. Interestingly, this complex shows hysteresis below 3 K at a sweep rate of 235 mTs^{-1} (Fig. 12). The coercivity of the hysteresis loops increases with decreasing temperature and increasing field

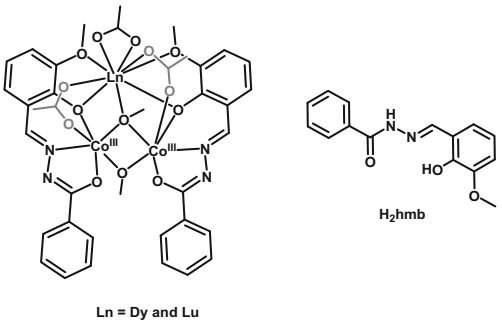

Fig. 10 Line diagram of complexes **26** and **27** along with the ligand

Table 3 Magnetic data of **t**rinuclear Co(II)−Ln(III) SMMs

Molecular formula[a]	U_{eff} (K), H_{DC} (Oe)	τ_0 (s)	Ref.
$[Co^{II}_2Ln(Hvab)_4(NO_3)](NO_3)_2$ Ln = Sm (**28**), Gd (**29**), Tb (**30**) and Dy (**31**)	No peak maxima under zero DC field		[40]
$[Co^{II}_2Dy(LH_3)_4](NO_3)_3$ (**32**)	No peak maxima under zero DC field		[41]
$\{[Co^{II}Dy_2(BPDC)_4(H_2O)_6]\cdot xH_2O\}_n$ (**33**)	3[b], 0	10^{-6}	[42]
$[Co^{II}_2GdL_2^{benzi}](NO_3)$ (**34**)	21.3, 0[c]	1.52×10^{-7}[c]	[43]
	18.9, 3,000	2.0×10^{-7}	
$[Co^{II}_2TbL_2^{benzi}]NO_3$ (**35**)	14.5, 0[c]	3.0×10^{-6}[c]	[43]
	20.9, 3,000	3.4×10^{-6}	
$[Co^{II}_2DyL_2^{benzi}]NO_3$ (**36**)	[c]	[c]	[43]
$[Co^{III}_2Dy(valdien)_2(OCH_3)_2(chp)_2](ClO_4)$ (**37**)	71.4, 2,000	5.6×10^{-6}	[44]
$[Co^{III}_2Tb(valdien)_2(OCH_3)_2(chp)_2](ClO_4)$ (**38**)	32.3, 2,000	2.5×10^{-10}	[44]

[a] *H_2vab* 2-[(2-hydroxymethyl-phenylimino)-methyl]-6-methoxyphenol, *LH_4* 2-(2-hydroxy-3-(hydroxymethyl)-5-methylbenzylideneamino)-2-methylpropane1,3-diol, *H_2BPDC* 2,2′-bipyridine-3,3′-dicarboxylic acid, *$H_2valdien$* *N*1,*N*3-bis(3-methoxysalicylidene)diethylenetriamine, *Hchp* 6-chloro-2-hydroxypyridine, *H_3L^{benzi}* *N*,*N*′,*N*″-tris(2-hydroxy-3-methoxybenzilidene)-2-(aminomethyl)-2-methyl-1,3-propanediamine

[b] $ln(\chi_M''/\chi_M') = ln(\omega\tau_0) + E_a/k_BT$

[c] Show hysteresis loops below 1.1 K

sweep rate. The loops display steplike features below 1.5 K, indicating the possibility of resonant QTM below this temperature.

Replacement of the solvent molecules coordinated with the Co^{2+} centers to form $[Co^{II}_2Dy_2(L)_4(NO_3)_2(MeOH)_2]$ (**40**) and $[Co^{II}_2Dy_2(L)_4(NO_3)_2(DMF)_2]$ (**41**) did not affect the compounds from being SMMs [46]. An analogous Zn_2Dy_2 (**42**) complex has also been assembled. A comparison of the magnetic properties in the complexes **39**–**42** is given in Table 4 (Fig. 13).

A tetranuclear complex $[Co^{II}_2Dy_2(L)_4(NO_3)_2(DMF)_2]$ (**43**) possessing a butterfly/defect-dicubane topology such as described above could be obtained by

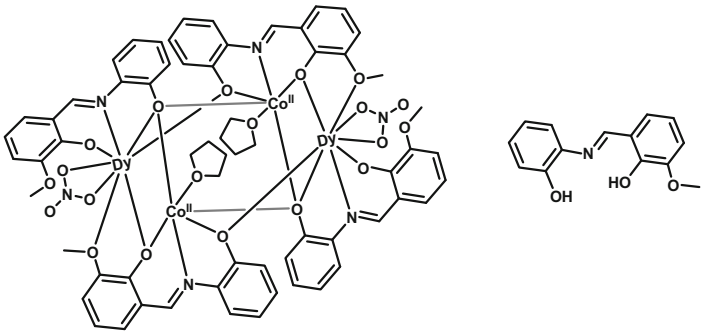

Fig. 11 Line diagram of complex **39** along with the ligand

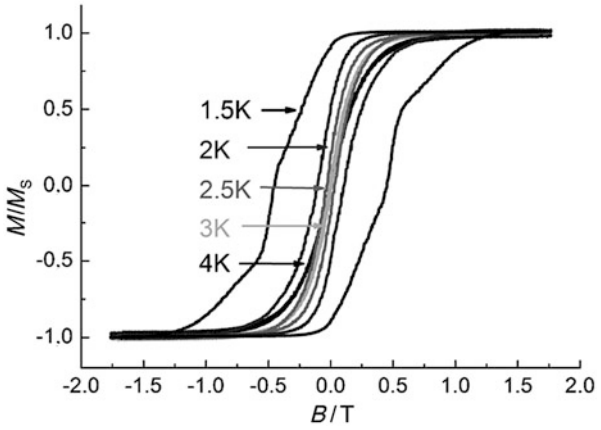

Fig. 12 Temperature-dependent magnetic hysteresis loops for **39** below 4 K with a sweep rate of 235 mTs^{-1}. Adapted from *Angew. Chem. Int. Ed.* **2012**, *51*, 7550–7554 with permission from John Wiley and Sons

the use of (*E*)-2-ethoxy-6-(((2-hydroxyphenyl)imino)methyl)phenol (H_2L) [47] (Fig. 14).

The magnetic properties of the [$Co^{II}_2Dy_2$] analogue and the analogous [$Dy_2Zn_2(L)_4(NO_3)_2(CH_3OH)_2$] (**44**) and [$Dy_2Mn^{III}_2(L)_4(NO_3)_2(DMF)_2$] (**45**) reveal that they are SMMs (Table 5).

The range of ligands that can afford tetranuclear complexes seem to be quite large. Thus, the complexes [$Co^{II}_2Ln_2(Hhms)_2(CH_3COO)_6(CH_3OH)_2(H_2O)_2$] ($NO_3$)$_2$[Ln = Dy^{III} (**46**), Gd^{III} (**47**), and Y^{III} (**48**)] could be prepared by using (2-hydroxy-3-methoxybenzylidene)-semicarbazide (H_2hms) [48] (Fig. 15).

Complex **46** shows temperature as well as frequency-dependent out-of-phase (χ'') signals ($\tau_0 = 6.4 \times 10^{-6}$ s; $U_{eff} = 6.7$ K at zero DC field; $\tau_0 = 3.2 \times 10^{-6}$ s and $U_{eff} = 13.8$ K at $H_{DC} = 800$ Oe in the range 2.0–5.5 K). Theoretical CASSCF calculation studies revealed that the Dy–Dy interactions are largely ferromagnetic

Table 4 Comparison of energy barriers for complexes $[Co_2Dy_2]$ (**39**–**41**) with the analogous $[Zn_2Dy_2]$ (**42**)

Complexes	THF-coordinated $[Co_2Dy_2]$ (**39**)	MeOH-coordinated $[Co_2Dy_2]$ (**40**)	DMF-coordinated $[Co_2Dy_2]$ (**41**)	$[Zn_2Dy_2]$ (**42**)
Barrier of Co^{II} –Dy^{III} (K)	15.8	17.9	17.5	–
Barrier of Dy^{III} (K)	118.1	104.8	94.5	140.4

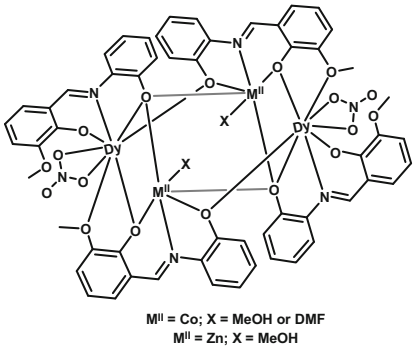

Fig. 13 Line diagram of complexes **40** and **41**

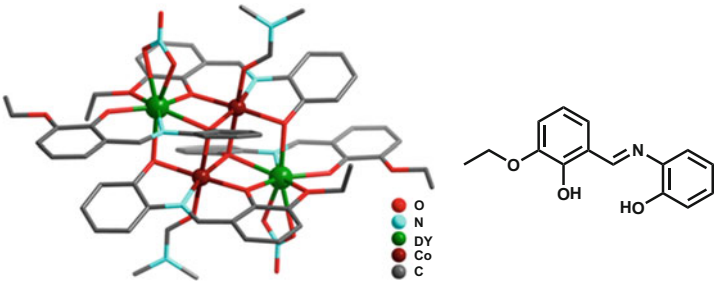

Fig. 14 Molecular structure complex **43** along with the ligand. Adapted from Ref. [47] with permission from The Royal Society of Chemistry

and dominant, while the exchange coupling (J_{exch}) of Dy–Co in $\{Co^{II}{}_2Dy^{III}{}_2\}$ is antiferromagnetic. Interestingly, in the analogous $\{Ni^{II}{}_2Dy^{III}{}_2\}$(**49**) complex, ferromagnetic exchange between Ni^{II} and Dy^{III} ions is found which is more conducive to zero-field single-molecule magnet behavior. The magnetic properties of tetranuclear complexes are summarized in Table 6.

Many tetranuclear complexes could also be assembled by the use of ethanolamine ligands. Thus, the complexes, $[Co^{III}{}_2Ln^{III}{}_2(OH)_2(bdea)_2(acac)_2(NO_3)_4]$ [Ln = Tb (**59**) and Dy(**60**)] and $bdeaH_2$ = *n*-butyldiethanolamine) containing two Co(III) ions, were prepared [57] (Fig. 16).

Table 5 Comparison of the AC magnetic data for $[Co^{II}_2Dy_2]$ with analogous $[M^{II}_2Dy_2]$ (M = Mn and Zn)

	Dy_2Zn_2 (1,000 Oe) (**44**)	Dy_2Mn_2 (0 Oe) (**45**)	Dy_2Co_2 (0 Oe) (**43**)	Dy_2Co_2 (1,000 Oe) (**43**)
τ_0/s	2.35×10^{-6}	1×10^{-8}	2.67×10^{-6}	8.77×10^{-7}
U_{eff}/K	115 (79.8 cm^{-1})	11 (7.6 cm^{-1})	125.1 (86.8 cm^{-1})	130 (99.4 cm^{-1})

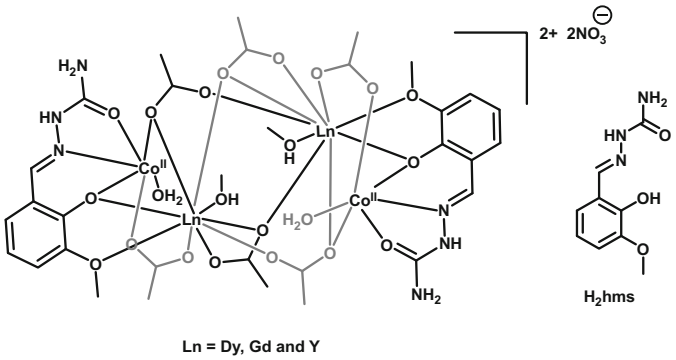

Fig. 15 Line diagram of complexes **46**–**48** along with the ligand

Table 6 Magnetic properties of representative tetranuclear $[Co_2Ln_2]$ SMMs

Molecular formula[a]	U_{eff} (K), H_{DC} (Oe)	τ_0 (s)	Ref.
$[Co^{II}_2Dy_2(pdmH)_4(Piv)_6]$ (**50**)	No maxima under zero DC field	–	[49]
$[Co^{II}_2Gd_2(ovan)_4(\mu_3\text{-}OH)_2(NO_3)_4]$ (**51**)	Hysteresis loops observed below 0.6 K	–	[50]
$[Co^{II}_2Ln_2(L^{bis\text{-}OMe})_2(PhCOO)_6(MeOH)_2]$ [Ln = Tb (**52**) and Dy (**53**)]	No maxima under zero DC field	–	[51]
$[Co^{II}_2Dy_2(\mu_3\text{-}OH)_2\text{-}(O_2C^tBu)_{10}](^iPr_2NH_2)_2$ (**54**)	No maxima under zero DC field	–	[52]
$[Co^{II}_2Dy_2(L^{di\text{-}Me})_2(PhCOO)_2(hfac)_4]$ (**55**)	8.8, 0	2.0×10^{-7}	[53]
	7.8, 1,000	3.9×10^{-7}	
$[Co^{III}Dy_3(HBpz_3)_6(dto)_3]$ (**56**)	52, 800	3.6×10^{-8}	[54]
$[Co^{III}_2Dy_2(L^{triamine})_2(CH_3COO)_4(OH)_2(H_2O)_2]\cdot(ClO_4)_2$ (**57**)	33.8, 0	3.73×10^{-6}	[55]
$[Co^{III}_2Dy_2(2,5\text{-}pydc)_6(H_2O)_4]_n$ (**58**)	4.89, 0	7.56×10^{-8}[b]	[56]

[a]*pdmH*$_2$ 2,6-pyridinedimethanol, *pivH* pivalic acid, *HBpz*$_3^-$ hydrotris(pyrazolyl)borate, *dto*$^{2-}$ dithiooxalatodianion ligand, *ovan* ortho-vanillin, *L*$^{bis\text{-}OMe}$*H*$_2$ 1,2-bis(2-hydroxy-3-methoxybenzylidene)hydrazine, *H*$_2$*L*$^{di\text{-}Me}$ *N*,*N*′-dimethyl-*N*,*N*′′-bis(2-hydroxy-3,5-dimethylbenzyl) ethylenediamine, *Hhfac* hexafluoroacetylacetone, *H*$_2$*L*^{triamine} *N*$_1$,*N*$_3$-bis(3-methoxysalicylidene) diethylenetriamine ligand, *2,5-pydc* 2,5-pyridine dicarboxylic acid

[b]SCM

Analysis of the AC susceptibility data for **60** allowed the extraction of the following parameters: $U_{eff} = 169$ K and $\tau_o = 1.47 \times 10^{-7}$ s above 20 K where the relaxation is thermally activated. As the temperature is decreased, a slight curvature appears in the Arrhenius plot of $\ln(\tau)$ vs $1/T$ but does not become

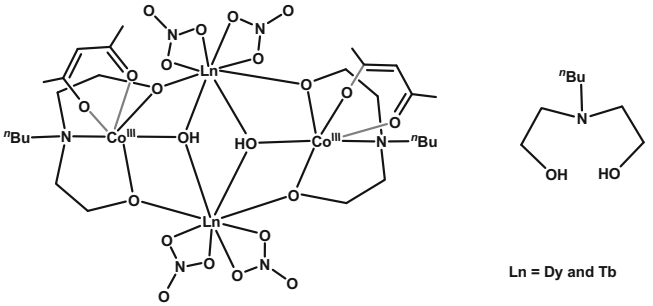

Fig. 16 Line diagram of complexes **59** and **60** along with the ligand

temperature independent at any point, indicating that a pure quantum regime is not observed within the timescale and temperature range of experiment. In contrast to complex **60**, **59** does not show SMM characteristics at zero DC field. However, upon application of 5,000 Oe DC field, a frequency-dependent maxima in the plot of χ_M'' vs T is seen. This phenomenon is a common feature for non-Kramers Tb^{III}-based complexes and is due to fast zero-field quantum tunneling of the magnetization between the sublevels. The non-Kramers ion generally allows the direct mixing of opposing projections of the ground state angular momentum/spin projections by the crystal field, so that tunneling pathways become readily accessible [58–63].

Other examples of tetranuclear heterometallic complexes [{$Ln^{III}_2Co^{III}_2(OMe)_2(teaH)_2(O_2CPh)_4(MeOH)_4$}$(NO_3)_2$][$Ln^{III}_2Co^{III}_2(OMe)_2(teaH)_2(O_2CPh)_4(MeOH)_2(NO_3)_2$] [Ln = Gd (**61**), Tb (**62**) and Dy (**63**)] were prepared using triethanolamine ($teaH_3$). Interestingly two tetranuclear units containing [$Ln^{III}_2Co^{III}_2(OMe)_2(teaH)_2(O_2CPh)_4(MeOH)_4](NO_3)_2$ and [$Ln^{III}_2Co^{III}_2(OMe)_2(teaH)_2(O_2CPh)_4(MeOH)_2(NO_3)_2$] are present within the same crystal [64] (Fig. 17).

AC susceptibility measurements in a zero DC field reveal the SMM behavior for the Dy^{III} analogue with the following characteristics above 8.5 K: (U_{eff}) of 88.8 K (~61 cm^{-1}) and $\tau_0 = 5.64 \times 10^{-8}$ s. But below 8.5 K, the Arrhenius plot deviates slightly from linear behavior indicating the existence of QTM. However, applying field up to 1,000 Oe does not change significantly the peak maxima in the χ_M'' vs T plot, indicating that QTM is inefficient in this system.

Among other tetranuclear complexes assembled using triethanolamine as the ligand, containing two Co(III), are [$Dy^{III}_2Co^{III}_2(OMe)_2(teaH)_2(O_2CPh)_4(MeOH)_4$]$(NO_3)_2$ and [$Dy^{III}_2Co^{III}_2(OMe)_2(teaH)_2(O_2CPh)_4(MeOH)_2(NO_3)_2$] (**63**), [$Dy^{III}_2Co^{III}_2(OMe)_2(dea)_2(O_2CPh)_4(MeOH)_4](NO_3)_2$ (**64**), [$Dy^{III}_2Co^{III}_2(OMe)_2(mdea)_2(O_2CPh)_4(NO_3)_2$] (**65**), [$Dy^{III}_2Co^{III}_2(OMe)_2(bdea)_2(O_2CPh)_4(MeOH)_4](NO_3)_2$, and [$Dy^{III}_2Co^{III}_2(OMe)_2(bdea)_2(O_2CPh)_4(MeOH)_2(NO_3)_2$] (**66**) ($teaH_3$ = triethanolamine, $deaH_2$ = diethanolamine, $mdeaH_2$ = *N*-methyldiethanolamine, and $bdeaH_2$ = *N*-*n*-butyldiethanolamine). The extracted magnetic parameters, from the AC measurements of these complexes, are summarized in Table 7 [65].

In addition to the aforementioned complexes, complex [$Co^{III}_2Dy^{III}_2(OMe)_2(teaH)_2(Piv)_6$] (**67**) can also be prepared using triethanolamine ligand. This complex displays SMM behavior with $U_{eff} = 51$ K; $\tau_0 = 6.1 \times 10^{-7}$ s and

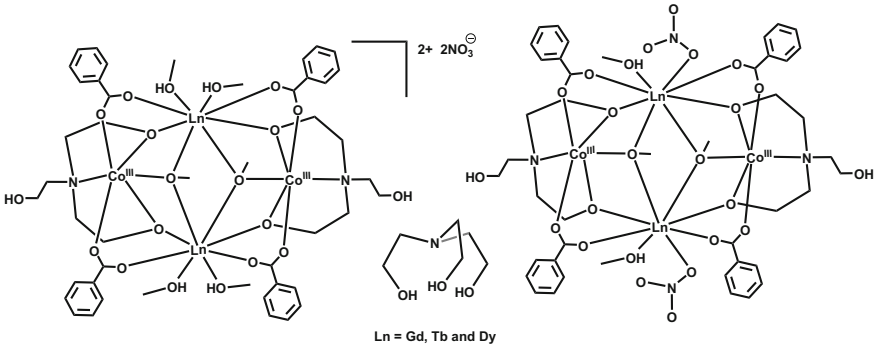

Fig. 17 Line diagrams of complexes **61**−**63** and the corresponding ligand

Table 7 Magnetic data for **63**–**66**

Complex	U_{eff} (cm^{-1})	Tunneling frequency (Hz)	τ_{QTM} (s)	τ_0 (s)	α
63	61	<0.1	>1.5	5.64×10^{-8}	0.29(4 K)–0.24(10.5 K)
64	72	1.29	0.12	6.05×10^{-8}	0.38(1.8 K)–0.28(12 K)
65	55	0.79	0.20	1.03×10^{-7}	0.42(1.8 K)–0.30(10.5 K)
66	80	0.34	0.48	3.38×10^{-8}	0.26(1.8 K)–0.15(14 K)

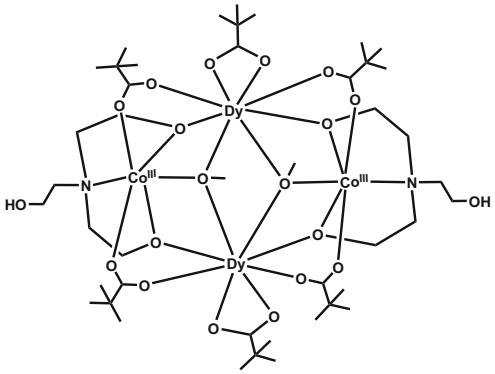

Fig. 18 Line diagram of complex **67**

τ_{QT} = 7.3 s in the range 4.5–7.5 K [U_{eff} = 127 K; $\tau_0 = 1.2 \times 10^{-9}$ s; $C_{Ram} = 1.7 \times 10^{-3}$ in the range of 7.5–9.5 K] [66] (Fig. 18).

For this complex, the energy level splitting under crystal field of the Dy^{III} ground J = 15/2 state was determined (Fig. 19). The thermal barrier for the fast relaxation pathways through $m_J = \pm 13/2$ and $m_J = \pm 11/2$ from ground state should be 39 and 104 cm^{-1}. These values compare quite well with the experimental U_{eff} = 35 cm^{-1} (51 K) and 88 cm^{-1} (127 K) values obtained from AC data (Fig. 20).

A summary of magnetization relaxation dynamics for this [$Co^{III}_2Ln^{III}_2$] family (**67**−**70**) is shown in Table 8 [67].

N-*n*-butyldiethanolamine ($bdeaH_2$) and *N*-methyldiethanolamine ($mdeaH_2$) were used as ligands for preparing [$Co_2^{III}Dy_2^{III}(OMe)_2(O_2CPh\text{-}2\text{-}Cl)_4(bdea)_2(NO_3)_2$]

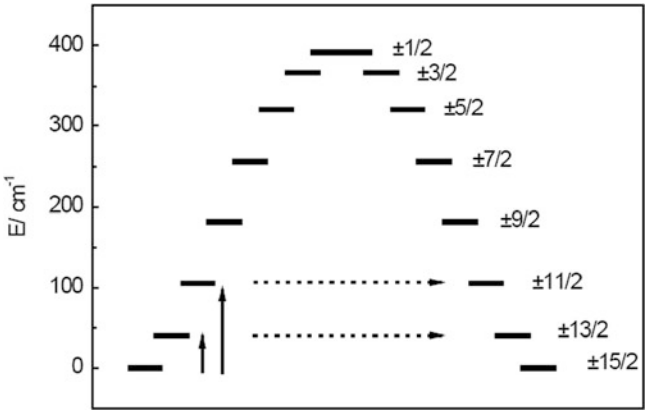

Fig. 19 Energy level splitting under crystal field of the Dy^{III} ground $J = 15/2$ state, with crystal field parameters, $B_0^2 = -2.4\ cm^{-1}$ $B_0^4 = 2.9 \times 10^{-3}\ cm^{-1}$. Arrows indicate the suggested relaxation pathways across the barrier. Adapted from Ref. [66] with permission from The Royal Society of Chemistry

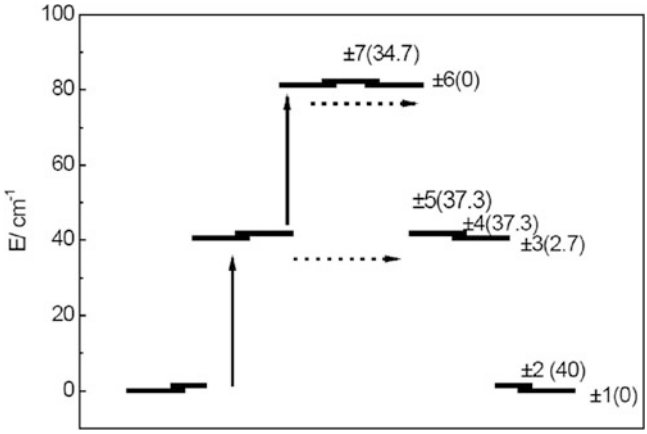

Fig. 20 Energy level splitting under crystal field of the Dy^{III} ground $J = 15/2$ state, with crystal field parameters, $B_0^2 = -2.4\ cm^{-1}$ $B_0^4 = 2.9 \times 10^{-3}\ cm^{-1}$ and exchange interaction $J_{exc} = -0.046\ cm^{-1}$. Arrows indicate the suggested relaxation pathways across the barrier. Doublets g_z^{eff} values between parentheses. Adapted from Ref. [66] with permission from The Royal Society of Chemistry

(**71**), $[Co_2^{III}Dy_2^{III}(OMe)_2(O_2CPh\text{-}4\text{-}^tBu)_4(bdea)_2(NO_3)(MeOH)_3](NO_3)$ (**72**), $[Co_2^{III}Co^{II}Ln^{III}(OH)(O_2CPh\text{-}4\text{-}OH)(bdea)_3(NO_3)_3(MeOH)]$ [Ln = Dy (**73**), Gd (**74**)], $[Co_2^{III}Dy_2^{III}(OMe)(OH)(O_2CPh\text{-}2\text{-}CF_3)_4(bdea)_2(NO_3)_2]$ (**75**), and $[Co_2^{III}Dy_2^{III}(mdea)_4(hfacac)_3(O_2CCF_3)(H_2O)]$ (**76**) [68]. A summary of magnetization relaxation dynamics of these complexes (**71**−**76**) is enlisted in Table 9.

Similarly a series of SMMs $[Co^{III}{}_2Ln^{III}{}_2(\mu_3\text{-}OH)_2(o\text{-}tol)_4(mdea)_2(NO_3)_2]$ [Ln = Dy (**77**), Tb (**78**), Ho (**79**)] [69], $[Dy^{III}{}_2Co^{III}{}_2(OH)_2(teaH)_2(acac)_6]$ (**80**), $[Dy^{III}{}_2Co^{III}{}_2(OH)_2(bdea)_2(acac)_6]$(**81**), and $[Dy^{III}{}_2Co^{III}{}_2(OH)_2(edea)_2(acac)_6]$ (**82**) ($teaH_3$ = triethanolamine, $bdeaH_2$ = *N*-*n*-butyldiethanolamine, $edeaH_2$ = *N*-

Table 8 Magnetization dynamics data of complexes $[Co^{III}_2Ln^{III}_2]$ [67]

Complex	Mechanism	Parameters
$[Co^{III}_2Dy^{III}_2]$ (**67**) (zero DC field)	Orbach	$\tau_0 = 6.1 \times 10^{-7}$ s; $U_{eff} = 35$ cm^{-1}; $\tau_{QT} = 7.3$ s
	Orbach + Raman	$\tau_0 = 1.2 \times 10^{-9}$ s; $U_{eff} = 88$ cm^{-1}
$[Co^{III}_2Ho^{III}_2]$ (**68**) (1,500 Oe DC field)	Orbach	$\tau_0 = 6.2 \times 10^{-9}$ s;$U_{eff} = 30$ cm^{-1}
$[Co^{III}_2Er^{III}_2]$ (**69**) (3,000 Oe DC field)	Raman	$\tau^1_{QT} = 5.1 \times 10^{-3}$ s;$C_{Ram} = 3.5 \times 10^{-2}$ s^{-1} K^{-7} ($n = 7$);$\tau^2_{QT} = 0.103$ s
$[Co^{III}_2Yb^{III}_2]$ (**70**) (3,000 Oe DC field)	Orbach	$\tau_0 = 2.1 \times 10^{-6}$ s;$U_{eff} = 23$ cm^{-1} ;$\tau_{QT} = 1.3 \times 10^{-2}$ s

Table 9 Magnetization relaxation parameters for complexes **71–76**

	AC susceptibility data		
Complex	U_{eff} (applied field) (cm^{-1})	τ_o (s)	τ_{QTM} (s)
71	80.4 (0 Oe)	1.8×10^{-8}	0.9
72	76.9 and 95.6 (0 Oe)	3.8×10^{-9} and 5.6×10^{-8}	0.5 and n/a
73	117.4 (1,500 Oe)	3.4×10^{-7}	0.3
74	n/a	n/a	n/a
75	88.1 (0 Oe)	1.4×10^{-8}	~1.5
76	22.6 (0 Oe)	1.4×10^{-6}	0.004

ethyldiethanolamine and acacH = acetylacetone) [70] are reported. The detailed parameters associated with their SMM behavior are summarized in Table 10 (Fig. 21).

2.4 Higher Nuclearity Cobalt–Lanthanide SMMs

In this section we will deal with complexes whose nuclearity is greater than 4. Only representative examples will be discussed. The magnetic data for these complexes are tabulated in Table 11. A hexanuclear complex $[Dy_4Co^{III}_2(HL^2)_2(\mu_3\text{-}OH)_2(piv)_{10}(OH_2)_2]$ complex (**86**) was prepared by the use of 2-(2,3 dihydroxpropyliminomethyl)-6-methoxyphenol(H_3L^2) and pivalic acid as ligands. The molecule contains two dimeric Dy(III) sub-units on either side of a dimeric Co (III) motif. Each of the Co(III) centers along with a Dy(III) is involved in a defect cubane structural motif [83] (Fig. 22).

The field dependence of magnetization shows a rapid increase of M values at lower DC field, indicating the presence of intramolecular ferromagnetic interactions between spin carriers. The Arrhenius plot obtained from the frequency-dependent AC susceptibility measurements provides the signature of SMM with an energy gap (U_{eff}) of 18.4 cm^{-1} (26.47 K) and a pre-exponential factor $\tau_0 = 8.7 \times 10^{-6}$ s at $H_{DC} = 0$. The Cole–Cole plot provides the α value within the 0.19–0.13, indicating a single relaxation time is mainly involved and is independent of the temperature.

Table 10 Magnetization relaxation parameters on heterometallic $\{Co_2^{III}Dy_2^{III}\}$ butterfly SMMs, with the Dy^{III} ions in the body position, constructed with various ethanolamine-based ligands

Molecular formula[a]	U_{eff} (cm^{-1})	τ_{QTM} (s)	τ_0 (s)	Ref.
$[Co_2^{III}Dy_2^{III}(OH)_2(acac)_2(bdea)_2(NO_3)_4]$ (**60**)	117	>1.5	1.47×10^{-7}	[57]
$[Co_2^{III}Dy_2^{III}(OMe)_2(O_2CPh)_4(teaH)_2(MeOH)_4](NO_3)_2$ and $[Co_2^{III}Dy_2^{III}(OMe)_2(O_2CPh)_4(teaH)_2(NO_3)_2(MeOH)_2]$ (**63**)	61	>1.5	5.64×10^{-8}	[64, 65]
$[Co_2^{III}Dy_2^{III}(OMe)_2(O_2CPh)_4(dea)_2(MeOH)_4](NO_3)_2$ (**64**)	72	0.12	6.05×10^{-8}	[65]
$[Co_2^{III}Dy_2^{III}(OMe)_2(O_2CPh)_4(mdea)_2(NO_3)_2]$ (**65**)	55	0.2	1.03×10^{-7}	[65]
$[Co_2^{III}Dy_2^{III}(OMe)_2(O_2CPh)_4(bdea)_2(MeOH)_4](NO_3)_2$ and $[Co_2^{III}Dy_2^{III}(OMe)_2(O_2CPh)_4(bdea)_2(NO_3)_2(MeOH)_2]$ (**66**)	80	0.48	3.38×10^{-8}	[65]
$[Co_2^{III}Dy_2^{III}(OMe)_2(teaH)_2(piv)_6]$ (**67**)	35 and 88	7.3	6.1×10^{-7} and 1.2×10^{-9}	[66]
$[Co_2^{III}Dy_2^{III}(OMe)_2(O_2CPh\text{-}2\text{-}Cl)_4(bdea)_2(NO_3)_2]$ (**71**)	80	0.9	1.8×10^{-8}	[68]
$[Co_2^{III}Dy_2^{III}(OMe)_2(O_2CPh\text{-}4\text{-}^tBu)_4(bdea)_2(NO_3)(MeOH)_3](NO_3)]$ (**72**)	77 and 96	0.5	3.8×10^{-9} and 5.6×10^{-8}	[68]
$[Co_2^{III}Co^{II}Dy^{III}(OH)(O_2CPh\text{-}4\text{-}OH)(bdea)_3(NO_3)_3(MeOH)]$ (**73**)	117	0.3 (1,500 Oe)	3.4×10^{-7}	[68]
$[Co_2^{III}Dy_2^{III}(OMe)_2(O_2CPh\text{-}2\text{-}CF_3)_4(bdea)_2(NO_3)_2]$ (**75**)	88	~1.5	1.4×10^{-8}	[68]
$[Co_2^{III}Dy_2^{III}(mdea)_4(hfacac)_3(O_2CCF_3)(H_2O)]$ (**76**)	23	0.004	1.4×10^{-6}	[68]
$[Co^{III}{}_2Dy^{III}{}_2(\mu_3\text{-}OH)_2(o\text{-}tol)_4(mdea)_2(NO_3)_2]$ (**77**)	81.2	0.34	9.8×10^{-9}	[69]
$[Co^{III}{}_2Dy^{III}{}_2(OH)_2(teaH)_2(acac)_6]$ (**80**)	49 and 31	76.5	2.7×10^{-7} and 3.2×10^{-7}	[70]
$[Co^{III}{}_2Dy^{III}{}_2(OH)_2(bdea)_2(acac)_6]$ (**81**)	19	1.4 ms	1.0×10^{-6}	[70]
$[Co^{III}{}_2Dy^{III}{}_2(OH)_2(edea)_2(acac)_6]$ (**82**)	11	[b]	1.3×10^{-6}	[70]
$[Co_2^{III}Dy_2^{III}(OMe)_2(acac)_4(mdea)_2(NO_3)_2]$ (**83**)	26	0.0025	2.6×10^{-6}	[71]
$[Co_2^{III}Dy_2^{III}(OMe)_2(acac)_4(teaH)_2(NO_3)_2]$ (**84**)	19	0.00058	8.1×10^{-6}	[71]
$[Co^{III}{}_2Dy^{III}{}_2(OH)_2(teaH)_2(acac)_4(NO_3)_2]$ (**85**)	20	0.00058	7.4×10^{-6}	[71]

[a]*deaH*$_2$ diethanolamine, *teaH*$_3$ triethanolamine, *bdeaH*$_2$ *N-n*-butyldiethanolamine, *edeaH*$_2$ *N*-ethyldiethanolamine, *mdeaH*$_2$ *N*-methyldiethanolamine, *o-tol* *o*-toluate, *pivH* pivalic acid, *acac* acetylacetonate, *hfacac* hexafluroacetylacetonate

[b]Denotes no pure quantum tunneling relaxation regime is observed above 1.8 K

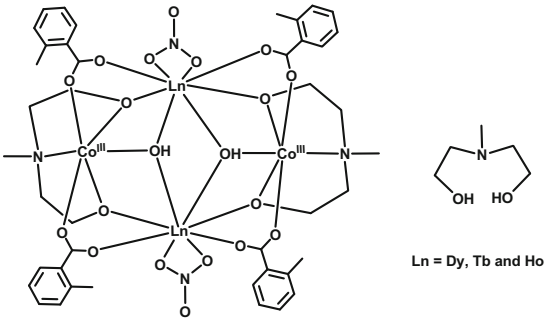

Fig. 21 Line diagram of complexes **77**–**79** along with the ligand

Table 11 Magnetic properties of high nuclearity Co^{II}/Ln^{III} SMMs

Molecular formula[a]	U_{eff} (K), H_{DC} (Oe)	τ_0 (s)	Ref.
$\{[Co^{II}_2Dy_3(BPDC)_5(HBPDC)(H_2O)_5](ClO_4)_2{\cdot}mH_2O\}_n$ (**90**)	62.89, 5,000	6.16×10^{-8}	[72]
$\{[Co^{II}_4Dy_2(L^{terpy})_4(CO_3)_4(HCOO)_2(H_2O)_2]{\cdot}2DMF{\cdot}xH_2O\}_n$ (**91**)	7.6, 5,000	1.9×10^{-6}	[73]
$[Co^{II}_6Dy(aib)_6(OH)_3(NO_3)_3(CH_3OH)_5(H_2O)](ClO_4)_3$ (**92**)	No maxima under zero DC field	–	[74, 75]
$[Co^{II}_6Dy_2(OH)_4(chp)_6(piv)_8(CH_3CN)_2]$ (**93**)	7.7, 1,000	5.7×10^{-8b}	[76]
$[Co^{II}_4Dy_4(OH)_4(chp)_{10}(acac)_6]$ (**94**)	No maxima under zero DC field	–	[77]
$[Co^{II}_{11}Dy_6(OH)_{14}(chp)_{14}(piv)_8(NO_3)_4(MeCN)_4]$ (**95**)	No maxima under zero DC field	–	[77]
$[Co^{II}_2Co^{III}_4Dy_4(Htris)_8(OAc)_6(NO_3)_4(L)_2](NO_3)_2$ (**96**)	No maxima under zero DC field	–	[78]
$[Co^{II}_3Co^{III}_2Dy_3(\mu_3\text{-}OH)_5(O_2C^tBu)_{12}(L^{Bu})_2]$ (**97**)	3.8, 2,000	1.5×10^{-6}	[79]
$[Co^{III}_2Dy_4(\mu_3\text{-}OH)_2(hmp)_4(\mu\text{-}N_3)_2\text{-}(piv)_8(NO_3)_2]$ (**98**)	3.8, 600	4.8×10^{-6}	[80]
$[Co^{III}_2Dy_4(\mu_3\text{-}OH)_2(salpa)_4(NO_3)_4(OAc)_4(H_2O)_2]$ (**99**)	2, 0	10^{-6b}	[81]
$[(Co^{III}_3Dy_3(\mu_3\text{-}OH)_4(O_2C^tBu)_6(L^{Bu})_3](NO_3)_2$ (**100**)	17.4, 2,000	2.5×10^{-6}	[79]
$[Co^{III}_2Dy_4(\mu_3\text{-}OH)_2(piv)_4(hmmp)_4(ae)_2]{\cdot}(NO_3)_2$ (**101**)	25.2, 5,000	1.3×10^{-6}	[82]
	32.4, 8,000	4.2×10^{-7}	

[a]*BPDC* 5,5′-dicarboxylate-2,2′-dipyridine anion, *Hhmp* 2-(hydroxymethyl)pyridine, $L^{terpy}H$ 4′-(4-Carboxyphenyl)-2,2′:6′,2″-terpyridine, H_3L^2 2-(2,3-dihydroxpropyliminomethyl)-6-methoxyphenol, H_2hmmp 2-[(2-hydroxyethylimino)methyl]-6-methoxyphenol, *Hae* 2-amino ethanol, *Hpiv* pivalic acid, H_2L^{Bu} *n-N*-butyldiethanolamine, *aibH* 2-amino-isobutyric acid, *Hchp* 6-chloro-2-pyridinol, $acac^-$ acetylacetonate, H_3tris *tris*-(hydroxymethyl)aminomethane

[b]$ln(\chi''_M/\chi'_M) = ln(\omega\tau_0) + E_a/k_BT$

Two octanuclear complexes, $[Co^{III}_4Dy_4(\mu\text{-}OH)_4(\mu_3\text{-}OMe)_4\{O_2CC(CH_3)_3\}_4(tea)_4(H_2O)_4]$ (**87**) and $[Co^{III}_4Dy^{III}_4(\mu\text{-}F)_4(\mu_3\text{-}OH)_4(o\text{-}tol)_8(mdea)_4]$ (**88**) (tea^{3-} = triply deprotonated triethanolamine; $mdea^{2-}$ = doubly deprotonated *N*-

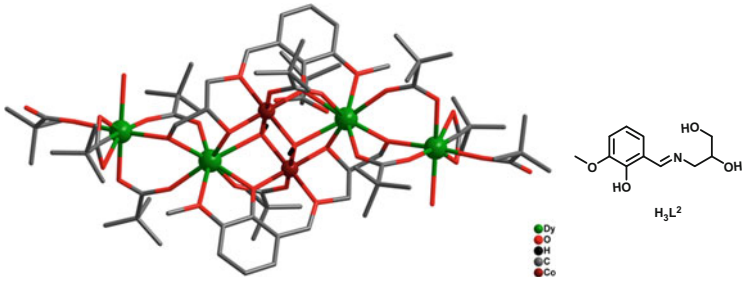

Fig. 22 Molecular structure of complex **86** along with the ligand. Adapted from Ref. [83] with permission from The Royal Society of Chemistry

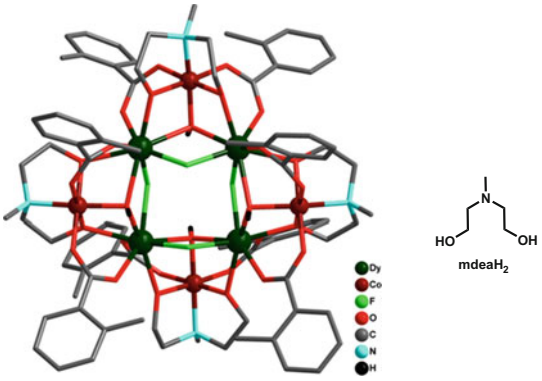

Fig. 23 Molecular structure of complex **88** along with the ligand. Adapted from *Chem. Eur. J.* **2017**, *23*, 1654–1666 with permission from John Wiley and Sons

methyldiethanolamine; *o*-tol = *o*-toluate), have been recently reported. The central core of the octanuclear ensemble consists of a $[Dy(III)]_4$ motif and is surrounded by four Co(III) ions. Like in the previous case, each of the Co(III) along with two Dy (III) centers is involved in a defect cubane motif [84] (Fig. 23).

Complex **87** reveals frequency-dependent "tails" in the out-of-phase susceptibility against temperature plots below 3 K at $H_{DC} = 0$ Oe. This behavior does not improve even after application of fields up to 5,000 Oe. But for complex **88**, at $H_{DC} = 5{,}000$ Oe, the corresponding energy barrier $U_{eff} = 39$ cm^{-1} and pre-exponential factor $\tau_0 = 1.0 \times 10^{-6}$ s can be obtained between 8 and 10.5 K.

A dodecanuclear complex $[Co^{II}_2Dy_{10}(L)_4(OAc)_{16}(SCN)_2(CH_3CN)_2(H_2O)_4(OH)_2(\mu_3\text{-}OH)_4][Co(SCN)_4(H_2O)]_2$ (**89**) was assembled by using the multifunctional ligand, 1,2-bis(2-hydroxy-3-methoxybenzylidene) hydrazine (H_2L). In contrast to the examples discussed above, this complex contains Co(II) [85] (Fig. 24).

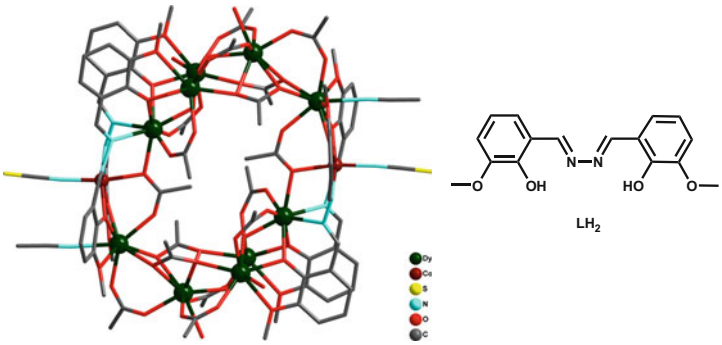

Fig. 24 Molecular structure of complex **89** along with the ligand. Adapted from Ref. [85] with permission from The Royal Society of Chemistry

The nature of the Co^{II}–Dy and Dy–Dy interactions could not be delineated with certainty. However, the authors, based on the AC susceptibility measurements, suggest that this complex has a SMM behavior.

3 Summary

Co(II) is a promising 3d metal ion with first-order orbital contribution that has been investigated for its interesting magnetic properties. The combination of Co(II) and lanthanide ions in the form of heterometallic complexes leads to an interesting array of complexes where the role of the ligand seems to be extremely crucial in modulating the nuclearity and the coordination geometry. While there has been considerable progress in this field, it is anticipated that appropriate design of complexes can lead to SIMs and SMMs with even better properties. One crucial element that is missing from the studies carried out so far seems to be a strong theoretical input. Once such an understanding is in place, it becomes easier for synthetic chemists to make appropriate designs for assembling SMMs with superior properties.

References

1. Murrie M (2010) Chem Soc Rev 39:1986–1995
2. Craig GA, Murrie M (2015) Chem Soc Rev 44:2135–2147
3. Frost JM, Harriman KLM, Murugesu M (2016) Chem Sci 7:2470–2491
4. Ishikawa N, Sugita M, Ishikawa T, Koshihara S-Y, Kaizu Y (2003) J Am Chem Soc 125:8694–8695
5. Osa S, Kido T, Matsumoto N, Re N, Pochaba A, Mrozinski J (2004) J Am Chem Soc 126:420–421
6. Bencini A, Benelli C, Caneschi A, Carlin RL, Dei A, Gatteschi D (1985) J Am Chem Soc 107:8128–8136

7. Woodruff DN, Winpenny REP, Layfield RA (2013) Chem Rev 113:5110–5148
8. Langley SK, Wielechowski DP, Chilton NF, Moubaraki B, Murray KS (2015) Inorg Chem 54:10497–10503
9. Langley SK, Wielechowski DP, Vieru V, Chilton NF, Moubaraki B, Abrahams BF, Chibotaru LF, Murray KS (2013) Angew Chem Int Ed 52:12014–12019
10. Ahmed N, Das C, Vaidya S, Langley SK, Murray KS, Shanmugam M (2014) Chem Eur J 20:14235–14239
11. Rinehart JD, Fang M, Evans WJ, Long JR (2011) Nat Chem 3:538
12. Rinehart JD, Fang M, Evans WJ, Long JR (2011) J Am Chem Soc 133:14236–14239
13. Pasatoiu TD, Sutter J-P, Madalan AM, Fellah FZC, Duhayon C, Andruh M (2011) Inorg Chem 50:5890–5898
14. Winpenny REP (1998) Chem Soc Rev 27:447–452
15. Benelli C, Gatteschi D (2002) Chem Rev 102:2369–2388
16. Mishra A, Wernsdorfer W, Abboud KA, Christou G (2004) J Am Chem Soc 126:15648–15649
17. Tanase S, Reedijk J (2006) Coord Chem Rev 250:2501–2510
18. Andruh M, Costes J-P, Diaz C, Gao S (2009) Inorg Chem 48:3342–3359
19. Sessoli R, Powell AK (2009) Coord Chem Rev 253:2328–2341
20. Karotsis G, Kennedy S, Teat SJ, Beavers CM, Fowler DA, Morales JJ, Evangelisti M, Dalgarno SJ, Brechin EK (2010) J Am Chem Soc 132:12983–12990
21. Papatriantafyllopoulou C, Wernsdorfer W, Abboud KA, Christou G (2011) Inorg Chem 50:421–423
22. Sharples JW, Collison D (2014) Coord Chem Rev 260:1–20
23. Rosado Piquer L, Sanudo EC (2015) Dalton Trans 44:8771–8780
24. Chandrasekhar V, Pandian BM, Azhakar R, Vittal JJ, Clérac R (2007) Inorg Chem 46:5140–5142
25. Chandrasekhar V, Pandian BM, Vittal JJ, Clérac R (2009) Inorg Chem 48:1148–1157
26. Chorazy S, Rams M, Nakabayashi K, Sieklucka B, Ohkoshi S-I (2016) Chem Eur J 22:7371–7375
27. Colacio E, Ruiz J, Ruiz E, Cremades E, Krzystek J, Carretta S, Cano J, Guidi T, Wernsdorfer W, Brechin EK (2013) Angew Chem Int Ed 52:9130–9134
28. Palacios MA, Nehrkorn J, Suturina EA, Ruiz E, Gómez-Coca S, Holldack K, Schnegg A, Krzystek J, Moreno JM, Colacio E (2017) Chem Eur J 23:11649–11661
29. Xie Q-W, Wu S-Q, Shi W-B, Liu C-M, Cui A-L, Kou H-Z (2014) Dalton Trans 43:11309–11316
30. Towatari M, Nishi K, Fujinami T, Matsumoto N, Sunatsuki Y, Kojima M, Mochida N, Ishida T, Re N, Mrozinski J (2013) Inorg Chem 52:6160–6178
31. Wang X, Li H, Sun J, Yang M, Li C, Li L (2017) New J Chem 41:2973–2979
32. Dolai M, Ali M, Titis J, Boca R (2015) Dalton Trans 44:13242–13249
33. Hazra S, Titis J, Valigura D, Boca R, Mohanta S (2016) Dalton Trans 45:7510–7520
34. Bartolomé J, Filoti G, Kuncser V, Schinteie G, Mereacre V, Anson CE, Powell AK, Prodius D, Turta C (2009) Phys Rev B 80:014430
35. Goura J, Brambleby J, Goddard P, Chandrasekhar V (2015) Chem Eur J 21:4926–4930
36. Goura J, Brambleby J, Topping CV, Goddard PA, Suriya Narayanan R, Bar AK, Chandrasekhar V (2016) Dalton Trans 45:9235–9249
37. Li X-L, Min F-Y, Wang C, Lin S-Y, Liu Z, Tang J (2015) Inorg Chem 54:4337–4344
38. Guo Y-N, Xu G-F, Wernsdorfer W, Ungur L, Guo Y, Tang J, Zhang H-J, Chibotaru LF, Powell AK (2011) J Am Chem Soc 133:11948–11951
39. Xue S, Ungur L, Guo Y-N, Tang J, Chibotaru LF (2014) Inorg Chem 53:12658–12663
40. Modak R, Sikdar Y, Thuijs AE, Christou G, Goswami S (2016) Inorg Chem 55:10192–10202
41. Chandrasekhar V, Das S, Dey A, Hossain S, Kundu S, Colacio E (2014) Eur J Inorg Chem 2014:397–406
42. Zhou J-M, Shi W, Xu N, Cheng P (2013) Cryst Growth Des 13:1218–1225

43. Yamaguchi T, Costes J-P, Kishima Y, Kojima M, Sunatsuki Y, Bréfuel N, Tuchagues J-P, Vendier L, Wernsdorfer W (2010) Inorg Chem 49:9125–9135
44. Liu C-M, Zhang D-Q, Hao X, Zhu D-B (2014) Chem Asian J 9:1847–1853
45. Mondal KC, Sundt A, Lan Y, Kostakis GE, Waldmann O, Ungur L, Chibotaru LF, Anson CE, Powell AK (2012) Angew Chem Int Ed 51:7550–7554
46. Peng Y, Mereacre V, Anson CE, Powell AK (2017) Dalton Trans 46:5337–5343
47. Li J, Wei R-M, Pu T-C, Cao F, Yang L, Han Y, Zhang Y-Q, Zuo J-L, Song Y (2017) Inorg Chem Front 4:114–122
48. Wu H, Li M, Zhang S, Ke H, Zhang Y, Zhuang G, Wang W, Wei Q, Xie G, Chen S (2017) Inorg Chem 56:11387–11397
49. Zhao X-Q, Lan Y, Zhao B, Cheng P, Anson CE, Powell AK (2010) Dalton Trans 39:4911–4917
50. Costes J-P, Vendier L, Wernsdorfer W (2011) Dalton Trans 40:1700–1706
51. Wu J, Zhao L, Zhang P, Zhang L, Guo M, Tang J (2015) Dalton Trans 44:11935–11942
52. Moreno Pineda E, Chilton NF, Tuna F, Winpenny REP, McInnes EJL (2015) Inorg Chem 54:5930–5941
53. Abtab SMT, Majee MC, Maity M, Titiš J, Boča R, Chaudhury M (2014) Inorg Chem 53:1295–1306
54. Xu G-F, Gamez P, Tang J, Clérac R, Guo Y-N, Guo Y (2012) Inorg Chem 51:5693–5698
55. Zhao L, Wu J, Xue S, Tang J (2012) Chem Asian J 7:2419–2423
56. Huang Y-G, Wang X-T, Jiang F-L, Gao S, Wu M-Y, Gao Q, Wei W, Hong M-C (2008) Chem Eur J 14:10340–10347
57. Langley SK, Chilton NF, Moubaraki B, Murray KS (2013) Chem Commun 49:6965–6967
58. Rinehart JD, Long JR (2011) Chem Sci 2:2078–2085
59. Sorace L, Benelli C, Gatteschi D (2011) Chem Soc Rev 40:3092–3104
60. Bar AK, Pichon C, Sutter J-P (2016) Coord Chem Rev 308:346–380
61. Habib F, Murugesu M (2013) Chem Soc Rev 42:3278–3288
62. Zhang P, Guo Y-N, Tang J (2013) Coord Chem Rev 257:1728–1763
63. Gómez-Coca S, Aravena D, Morales R, Ruiz E (2015) Coord Chem Rev 289-290:379–392
64. Langley SK, Chilton NF, Ungur L, Moubaraki B, Chibotaru LF, Murray KS (2012) Inorg Chem 51:11873–11881
65. Langley SK, Ungur L, Chilton NF, Moubaraki B, Chibotaru LF, Murray KS (2014) Inorg Chem 53:4303–4315
66. Funes AV, Carrella L, Rentschler E, Albores P (2014) Dalton Trans 43:2361–2364
67. Funes AV, Carrella L, Rechkemmer Y, van Slageren J, Rentschler E, Albores P (2017) Dalton Trans 46:3400–3409
68. Langley SK, Le C, Ungur L, Moubaraki B, Abrahams BF, Chibotaru LF, Murray KS (2015) Inorg Chem 54:3631–3642
69. Vignesh KR, Langley SK, Murray KS, Rajaraman G (2017) Inorg Chem 56:2518–2532
70. Langley SK, Chilton NF, Moubaraki B, Murray KS (2015) Inorg Chem Front 2:867–875
71. Langley SK, Chilton NF, Moubaraki B, Murray KS (2013) Inorg Chem 52:7183–7192
72. Fang M, Shi P-F, Zhao B, Jiang D-X, Cheng P, Shi W (2012) Dalton Trans 41:6820–6826
73. Liu Y, Chen Z, Ren J, Zhao X-Q, Cheng P, Zhao B (2012) Inorg Chem 51:7433–7435
74. Orfanoudaki M, Tamiolakis I, Siczek M, Lis T, Armatas GS, Pergantis SA, Milios CJ (2011) Dalton Trans 40:4793–4796
75. Sopasis GJ, Orfanoudaki M, Zarmpas P, Philippidis A, Siczek M, Lis T, O'Brien JR, Milios CJ (2012) Inorg Chem 51:1170–1179
76. Zhao X-Q, Wang J, Bao D-X, Xiang S, Liu Y-J, Li Y-C (2017) Dalton Trans 46:2196–2203
77. Langley SK, Chilton NF, Moubaraki B, Murray KS (2013) Polyhedron 66:48–55
78. Xiang H, Lan Y, Li H-Y, Jiang L, Lu T-B, Anson CE, Powell AK (2010) Dalton Trans 39:4737–4739
79. Sheikh JA, Goswami S, Konar S (2014) Dalton Trans 43:14577–14585
80. Feuersenger J, Prodius D, Mereacre V, Clérac R, Anson CE, Powell AK (2013) Polyhedron 66:257–263

81. Jhan S-Y, Huang S-H, Yang C-I, Tsai H-L (2013) Polyhedron 66:222–227
82. Tian C-B, Yuan D-Q, Han Y-H, Li Z-H, Lin P, Du S-W (2014) Inorg Chem Front 1:695–704
83. Zou H-H, Sheng L-B, Liang F-P, Chen Z-L, Zhang Y-Q (2015) Dalton Trans 44:18544–18552
84. Vignesh KR, Langley SK, Murray KS, Rajaraman G (2017) Chem Eur J 23:1654–1666
85. Zou L-F, Zhao L, Guo Y-N, Yu G-M, Guo Y, Tang J, Li Y-H (2011) Chem Commun 47:8659–8661